Collapse of transient gels in colloid-polymer mixtures

2002 J. Phys.: Condens. Matter 14 2485

(http://iopscience.iop.org/0953-8984/14/10/302)

INSTITUTE OF PHYSICS PUBLISHING JOURNAL OF PHYSICS: CONDENSED MATTER

J. Phys.: Condens. Matter **14** (2002) 2485–2505 PII: S0953-8984(02)31125-1

Collapse of transient gels in colloid–polymer mixtures

L Starrs[1,3], W C K Poon[1], D J Hibberd[2] and M M Robins[2]

[1] Department of Physics and Astronomy, The University of Edinburgh, Mayfield Road, Edinburgh EH9 3JZ, UK
[2] The Institute of Food Research, Norwich Research Park, Colney Lane, Norwich NR4 7UA, UK

Received 22 November 2001
Published 18 March 2002
Online at stacks.iop.org/JPhysCM/14/2485

Abstract

Transient gelation in colloid–polymer mixtures is an interesting but poorly understood non-equilibrium phenomenon which has recently attracted the attention of experiment and theory. In a transient gel the particles aggregate, by the depletion interaction, to form a space-spanning network which maintains its structural integrity for a finite period before suddenly collapsing. In this paper we present a study of the collapse process which provides new information on the way in which transient gels collapse. We have studied gel collapse in three ways. Firstly, we have observed the gel throughout its lifetime using dark-field optics and time-lapsed video recording. In a second experiment we have measured the concentration of gels throughout their entire height before, during and after collapse. This was performed using a non-intrusive ultrasonic technique which measures the speed of sound in the suspension. Finally, we have studied the effect of varying sample height and width on the lifetime of a gel. Our observations provide new information on the collapse process and have important implications for the formulation of a theoretical model. In discussing the effects of height and width we refer to the following companion paper which describes this particular effect.

1. Introduction

Transient gelation is an interesting non-equilibrium phenomenon found in many colloidal suspensions with weak, attractive interactions [1–4]. A transient gel is formed when the colloidal particles aggregate into a space-spanning network. This arrangement of colloids is not stable and the gel suddenly destabilizes after some finite time. The formation of these gels has been extensively studied by both experiment [2, 4–6] and theory [7–10]; however, the mechanism of their destabilization and collapse remains unclear. In this paper we address the problem of gel collapse by presenting a series of experimental observations made of this phenomenon.

[3] Current address: School of Chemistry, University of Bristol, Cantock's Close, Bristol BS8 1TS, UK.

A system commonly used to study transient gelation is the colloid–polymer mixture. Here non-adsorbing polymer is added to a colloidal suspension of hard spheres which can cause phase separation via the depletion mechanism [11]. The polymer coils and colloidal particles are mutually impenetrable and thus the polymer centres of mass are excluded from a distance around each colloidal particle of order r_g, the polymer radius of gyration. The polymer coils are restricted to the volume not occupied by colloidal particles and their depletion zones, the free volume V_{free}. The overlap of depletion layers of nearby particles creates more free volume for the polymer coils thus lowering the system's free energy by maximizing entropy. In this way, an effective attraction between the particles is induced which can be modelled by a pair potential, $U(r)$.

In practice we can explore the phase behaviour of a colloid–polymer system by varying $\xi = r_g/R$, where R is the radius of the colloidal particle, the colloid volume fraction ϕ and the polymer concentration C_p. Good agreement between the phase behaviour found by experiment and that predicted by theory in systems with a short interaction range has been observed [12, 13]. When a small amount of polymer is added no significant difference in the phase behaviour from that of a hard-sphere colloidal suspension is observed. Upon adding more polymer to the system it is found that the region of fluid–crystal coexistence is expanded as predicted by theory. However, at higher polymer concentrations crystallization is suppressed and a sequence of non-equilibrium behaviour, reminiscent of that found in the phase separation of simple liquids, is observed [2]. At the highest polymer concentrations the particles aggregate to form a space-filling gel that is transient in nature. Small-angle light scattering studies (SALS) [2] show that these gels are characterized by the presence of a ring of scattered intensity which remains static throughout a quiescent stage at $QR \sim 10^{-1}$, where Q is the scattering vector. Dynamic scaling of the maximum scattering intensity position at intermediate times during the assembly of the gel implies a fractal dimension of 1.7 for the particle network. After some time the scattering ring rapidly collapses to much lower angles ($QR \sim 10^{-2}$). This sudden collapse of the small-angle scattering ring coincides with the onset of rapid sedimentation of the gel.

It has been proposed that the crossover to a non-equilibrium regime corresponds to the dominance of particle aggregation over thermally driven rearrangements [2]. This can be modelled in the framework of diffusion-limited cluster aggregation with finite bond energies known as reversible DLCA [7]. In the DLCA model [14] strongly attracting particles explore space by diffusion forming permanent bonds upon touching. In three dimensions, DLCA produces clusters of particles with a fractal dimension of 1.8 which is consistent with the fractal dimension as determined from light scattering [2]. Gelation in the DLCA model occurs when the average particle volume fraction of a cluster is equal to the initial particle volume fraction. In reversible DLCA, interparticle bond strengths are of the order of a few k_BT and can be broken by thermal fluctuations with some finite probability. At high bond strengths reversible DLCA reproduces the behaviour of the DLCA model. However, at bond strengths of a few k_BT, we observe the formation of a space-spanning network which, once formed, breaks into large clusters and reforms many times. The structure is also more compact than the permanent gel formed by DLCA due to thermal fluctuations. This structure has been equated to that of the transient gel [7]. At bond strengths comparable with k_BT compaction due to thermal fluctuations dominates and the system can no longer span space. This crossover from a space-spanning structure to compact clusters can be used as an estimate of the position of the gelation boundary.

Until recently, studies of transient gelation have focused on the formation of the particle network; however, our current aim is to understand the mechanisms of destabilization and collapse of the gel. For the case where the density of the particles is greater than that

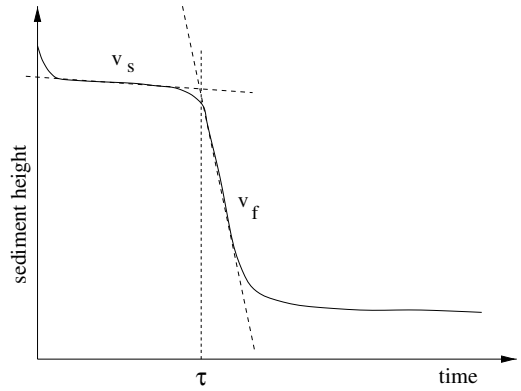

Figure 1. Schematic diagram of a height against time plot for a suspension exhibiting delayed sedimentation. The delay time, τ, and the slow and fast settling rates, v_s and v_f respectively, are shown.

of the suspending medium, transient gels exhibit a settling behaviour known as delayed sedimentation [15]. The defining characteristic of this behaviour is the presence of a delay time τ during which little or no settling is observed, before a sudden onset of rapid sedimentation. A plot of the height of the sediment interface $h(t)$ with time for a suspension exhibiting delayed sedimentation has a characteristic shape as shown in figure 1. From this plot we can extract information on the settling rate and delay time of a gel. The settling rates during the delay period and the rapid collapse stage, v_s and v_f respectively, can both be approximated by straight lines as shown in figure 1. The time coordinate of the intersection of these lines provides a measure of the delay time τ. Delayed sedimentation has been reported in many different colloidal systems [1,3,16,17]; however, it remains a poorly understood phenomenon.

Our current aim in studying transient gels is to understand the mechanisms of gel collapse. This is a phenomenon that is poorly understood but also inadequately defined. The picture of gel collapse in monodispersed systems under the influence of gravity is incomplete with many aspects appearing contradictory. The delay time of a gel has been found to depend on many parameters other than colloid and polymer concentration, including the height and width of the sample and its cross-sectional geometry [18, 19]. In this paper we present a collection of observations, on a set of transient gels with various lifetimes, which provide a more complete picture of the collapse process. Our study falls into three parts. Firstly, direct observations in the bulk of collapsing gels have been made using a dark-field imaging technique. These experiments have shown many new features in the collapse process and provide some insight into the physical processes involved. In the second experiment, the concentration of transient gels with height has been determined using a non-intrusive technique which measures the speed of ultrasound in the sample. The results of this study are consistent with the dark-field observations. Finally, we have studied the effect of sample height and width upon the measured delay time of a transient gel.

The remainder of this paper is structured in the following way. In section 2 we describe the three experimental techniques employed in this study of gel collapse. The results of each experiment are dealt with separately in section 3 and discussed in the context of each other in section 4. We shall also discuss the study of height and width dependence by referring to a theory presented in the following companion paper [19].

2. Experimental methods

2.1. Model system

The colloidal particles used were poly-methylmethacrylate (PMMA) spheres with radius $R = 186$ nm and size polydispersity $\sigma = \pm 5\%$. The particles were sterically stabilized by grafting a thin (10 mm) layer of poly-12-hydroxy-steric acid (PHSA) to the surface of the PMMA spheres. For the dark-field observations the particles were suspended in a mixture of tetrahydronapthalene (tetralin) and *cis*-decahydronapthalene (*cis*-decalin) which produced an ideal refractive index match between the particles and suspending solvent to give good dark-field imaging conditions. The non-adsorbing polymer added to the colloid was polystyrene (PS) which had a weight-averaged molecular mass of $M_w = 320\,000$ g mol^{-1} giving an estimated polymer radius of gyration of $r_g = 17$ nm [20] and a size ratio of $\xi \simeq 0.1$. The polydispersity in r_g was around 10%.

The same colloid–polymer system was used in the experiments to measure concentration profiles of collapsing gels using ultrasound and in the size dependence study. However, the suspending solvent was changed to pure *cis*-decalin. The composition of the suspending solvent was changed for two reasons. Firstly, refractive-index-matched samples were not required and secondly, it was found that tetralin significantly damaged the Perspex cells used in the ultrasonic experiments.

2.2. Dark-field observations

The turbidity of our samples has previously made it impossible to image in the bulk of the suspension. High-contrast imaging requires a large difference between the refractive indices of the particles and the suspending solvent. Unfortunately, this situation leads to a large amount of multiple scattering by the sample which makes imaging the bulk impossible. To reduce the amount of multiple scattering we combine two solvents (tetralin and *cis*-decalin) to match the refractive index of the solvent mixture to that of the particles. This creates poor contrast in the sample which is enhanced by using a dark-field imaging technique.

In order to form a dark-field image it is necessary to collect in the image plane only light that is scattered by the object. This condition for dark-field imaging may be achieved in a variety of ways [21] and we show in figure 2 a schematic diagram of the optical setup used in this study. Here, a collimated beam of white light illuminates the object. In our nearly indexed-matched samples, most of the light passes through the object undeviated forming a beam of unscattered light, as indicated by the solid rays in figure 2. Light weakly scattered by small refractive-index inhomogeneities in the sample fills the aperture of the objective lens and is collimated, dashed rays in figure 2. Under normal, bright-field, imaging conditions both scattered and unscattered rays are combined by the focusing lens to form an image. However, for the case of weak scattering, the unscattered light is many orders of magnitude higher in intensity than the scattered light. Thus the information contained in the scattered intensity is lost in a bright background of unscattered light. If the unscattered light is prevented from reaching the imaging plane then only the scattered light will be collected and a dark-field image can be formed. This is achieved by placing a small beamstop, 1–2 mm in diameter, in the back focal plane of the objective. Here the two beams are spatially separate and the unscattered light can be blocked without significantly reducing the intensity of the scattered radiation.

Our apparatus is similar in principle to a dark-field microscope [22] but differs in one crucial aspect. The objective and focusing lenses are chosen so as to create an image of reduced size: the optical magnification, given by $M = f_f/f_o$, is less than one. This is in order to fit an image of an entire sample, typically 2 cm high by 1 cm wide, onto the CCD array of

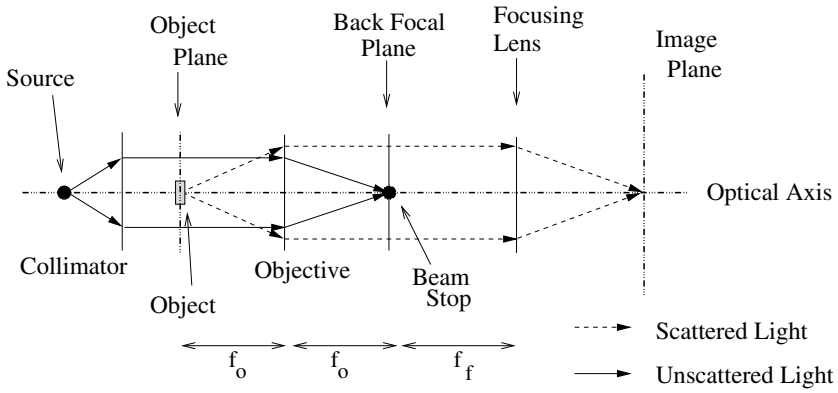

Figure 2. Schematic diagram showing the principle setup for dark-field imaging.

the camera used to capture the image. We are thus only able to image macroscopic features in our samples and it is for this reason that our apparatus is termed a dark-field macroscope.

In our macroscope only light which is forward scattered at an angle less than $\theta = 2.5^\circ$ ($QR \sim 0.1$) from the optical axis may enter the aperture of the lens and be detected. During the quiescent stage the gel scatters light at angles just outside the aperture of the lens. Thus, no scattered light is collected from a quiescent gel and it appears dark. As the gel collapses, scattering from broken fragments of the structure occurs at lower angles within the aperture of the lens. Thus the light scattered by broken gel structures is collected and so appears as a bright region. Solvent and polymer molecules are not visible using this technique as they scatter light very weakly and far outside the aperture of the objective due to their small size.

The sample cells used for the dark-field observations were of square cross-section (1 cm × 1 cm) and were typically 4 cm in height. They were sealed with a Teflon stopper which was fitted with an o-ring in order to reduce solvent evaporation. The cells were made of glass with four clear windows on the long dimension which were flat to within one micron. Typically a cell was filled to a height of 2 cm with the colloid–polymer sample. The sample was then mixed over a period of several hours by slow tumbling before being placed, as soon as possible after the cessation of mixing, into the dark-field macroscope.

Samples were prepared by firstly producing suspensions of colloid and polymer in the solvent mixture of known colloid volume fraction ϕ and polymer concentration C_p. Known masses of colloid and polymer solutions along with a known mass of excess solvent were then mixed in the sample cell to create a mixture of the desired composition (ϕ, C_p). Once sealed in the sample cell, the mixture was homogenized by slow tumbling over a period of hours. The relative errors in sample composition due to uncertainties in the concentrations of the solvent mixture, and polymer and colloid stock were estimated as $\Delta\phi/\phi = \pm 1\%$ and $\Delta C_p/C_p = \pm 2\%$.

2.3. Ultrasonic concentration profiles

In a second experiment we used a non-intrusive ultrasonic technique to measure the concentration of a gelled suspension during its collapse. The technique relies upon measuring the speed of an ultrasonic pulse as it travels through the suspension. The apparatus [23] determines the velocity of ultrasound in a dispersion from measurements of the time-of-flight of a pulse of ultrasound which can be determined to a precision of 5 ns in 25 μs. Two transducers

are mounted opposite each other on a rigid carriage which may be moved vertically up and down the sample by a stepper motor. The minimum step size is 1 mm. The transducers produce ultrasound with a typical centre frequency of 6.4 MHz corresponding to a wavelength in *cis*-decalin of around 224 μm at 20 °C. It should be noted that this technique is non-destructive and that the ultrasonic pulses do not disrupt the gel structure. The transducers produce an ultrasonic beam of estimated width 2 mm [24]. As only one pair of transducers is used we are unable to obtain an instantaneous measurement of time-of-flight throughout the whole sample and it can take up to 30 min for one scan to be completed. It is assumed that the concentration of the suspension is not significantly changing during this time.

A schematic diagram of the ultrasonic concentration profiling apparatus is shown in figure 3. To create a pulsed signal for the ultrasonic transducers, a function generator is used to produce a half sine wave. This signal is sent to a pulse generator which produces pulses at a frequency that can be continuously varied. The pulse output by the generator is then passed to the transmitter transducer via a linear amplifier. The signal received once it has travelled through the sample is passed from the receiving transducer through another linear amplifier to a calibrated attenuator. The two pulses are then compared, by eye, on an oscilloscope. To find the time-of-flight the time interval between the input pulses is varied. When the interval between transmitted pulses matches the time-of-flight, the transmitted pulse coincides on the oscilloscope screen with the received pulse from the previous transmission. The instrument is controlled by a microcomputer which is interfaced with a counter–timer and the stepper motor driving the transducer carriage. When the two pulses are made to coincide as described then the microcomputer is allowed to log the time-of-flight, the height of the transducers and the absolute time.

For these measurements the samples are contained in rectangular Perspex cells 14 mm wide by 10 mm deep by 192 mm high. The cell has two chambers which are separate from each other. The upper, larger chamber is where the sample is placed. The lower chamber, known as the false base, is filled with demineralized water and is used to make calibration measurements before each experimental run. The sample cell and the transducers are immersed in a temperature controlled water bath. This is necessary as the velocity of ultrasound in many substances is sensitive to temperature variations [25]. The water in the bath also acts to create a good ultrasonic contact between the transducers and the cell. Differences in the acoustic impedance of the sample cell material and the medium surrounding it cause losses in the transmitted signal due to reflection of the pulse at the interface. This creates extra pulses in the received signal which can mask the true signal.

Samples were prepared in glass 30 ml containers and slowly tumbled over a period of several hours until well mixed. The sample was then carefully loaded into the ultrasonic sample cell and immediately placed in the temperature bath of the apparatus. The sample was then allowed to stand in the bath at 25 $\pm$ 0.02 °C for 45 min before the first ultrasonic measurements were made. This was to allow the sample to reach a steady temperature.

The concentration of a suspension is related to the speed of sound in it by a quadratic relationship known as the Urick equation [26]

$$\left(\frac{v}{v_c}\right)^{-2} = \left[1 - \phi\left(1 - \frac{\rho_d}{\rho_c}\right)\right]\left[1 - \phi\left(1 - \frac{\rho_c v_c^2}{\rho_d v_d^2}\right)\right], \tag{1}$$

where v is the speed of ultrasound through the dispersion, v_c and v_d are the speeds of ultrasound through the continuous and dispersed phases respectively, ρ_c and ρ_d are the respective densities. This approach assumes that the dispersion can be treated as a simple mixture of its components which is valid in the limit of small particles in comparison with the wavelength of the ultrasound and a large difference in the speed of sound in the two components. The values of v_c, v_d, ρ_c

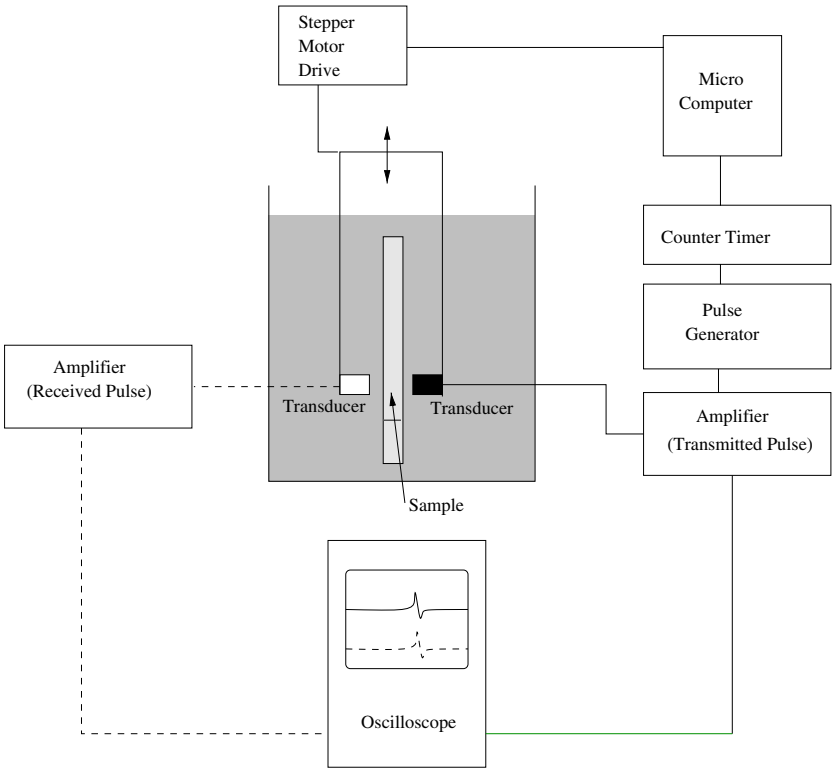

Figure 3. Schematic diagram of the apparatus to measure the velocity of ultrasound through colloidal dispersions.

and ρ_d are found by measuring the velocity of ultrasound in samples of pure colloid of known concentration. This produces some points on a calibration curve to which we fit a quadratic relationship in ϕ using v_c, v_d, ρ_c and ρ_d as parameters of the fit. By calibrating the system in this way the effects of low multiple scattering can be compensated for. The area under the concentration against height curve should remain constant with time since the mass of the system is conserved. This provides a check of the accuracy of the Urick calibration which is achieved by integrating the concentration against height data. For the samples presented in this paper, we have found a variation of 3–4% in the area under each curve.

2.4. Sedimentation profiles

The sedimentation profile (a plot of the height of the sediment top against time) has been determined for a transient gel for various initial heights $h(0)$ and widths. The sample under study had composition $\phi = 0.20$ and $C_p = 7.14$ mg cm^{-3}, which corresponds to a depletion potential of depth $U_0 \approx 6.5 k_B T$. Images of the settling behaviour were captured by a CCD video camera and recorded by a time-lapse video recorder under ambient lighting conditions. The sample was placed in a temperature-controlled heat bath at 25 °C. We have studied a range of initial heights, 5 mm $\leqslant h(0) \leqslant$ 100 mm. The sample cells had circular cross sections of diameter 5, 7, 10, 15, 20, 25 and 30 mm. The cells were made of glass and were sealed with a Teflon stopper fitted with an o-ring to minimize solvent evaporation. The sample was prepared in a similar way to those used in the dark-field observations.

3. Results

3.1. Direct observation

Figure 4 shows a time-lapsed sequence of dark-field images of a collapsing gel with a delay time of $\tau = 460$ min ($\sim$7 h). The sample shown here had a colloid volume fraction of 0.2 and polymer concentration 5.94 mg cm^{-3}. The initial height of the suspension was $h(0) = 24.5 \pm 0.1$ mm. The time at which images (*a*)–(*l*) were captured is shown on the sedimentation profile at the bottom of figure 4. In these pictures the very bottom of the sample has not been captured. Images (*m*)–(*o*) show a different gelled sample ($\phi = 0.19$, $C_p = 5.67$ mg cm^{-3} $\tau \sim 200$ min) where the initial suspension height was small enough to image the whole sample ($h(0) = 10$ mm).

Initially the whole sample appears dark except for small bright spots caused by dust on the inner surface of the sample cell, figure 4(*a*). During the delay period bright patches begin to form underneath the sample meniscus, figure 4(*b*), and grow across and downwards into the suspension. At the same time a layer of bright material begins to form at the bottom, figure 4(*m*). This grows steadily throughout the delay time, figure 4(*n*), and reaches a maximum thickness of around 1 mm.

Later in the delay 'channels' are observed travelling upwards in the sample. Figure 4(*c*) shows a channel that has just formed near the left-hand wall of the sample cell. Channels also appear bright and are observed to start at various points within the sample. Some observations have shown a tendency for channel formation to begin at or near the cell walls suggesting that they may nucleate on small inhomogeneities on the inner cell wall. More than one channel is often observed as is shown in figures 4(*d*) and (*e*) where two fainter, out of focus channels can be seen to the right of the first one. When a channel breaks through the surface of the suspension small volcano-like structures are observed as colloidal material carried by the channel is deposited. Once a channel breaks the surface of the suspension it begins to grow in width. The typical width of a channel initially is of order 0.5 mm which can increase to 2–3 mm before the onset of rapid collapse.

Figure 5(*a*) shows the variation of channel-front height with time for four different channels for a gel with a delay time of 460 min. The data are taken from two separate experiments run under the same conditions. The main feature of these curves is their apparent similarity in shape irrespective of the initial height and time. This is shown more clearly in figure 5(*b*) which shows the same curves shifted in height and time in order to make them collapse onto one master curve. By measuring the average slope of the channel height against time curves we have estimated the slow and fast propagation rates for the channels. The fast propagation rate of the channel $v_f^c = 2.1$ μm s^{-1} is of the same order of magnitude as the fast sedimentation speed $v_f = 0.8$ μm s^{-1} observed once the gel has begun rapid collapse. The slow channel propagation rate $v_s^c = 0.5$ μm s^{-1} is six times faster than the slow sedimentation rate $v_s = 0.08$ μm s^{-1}.

Approximately half way through the delay, the sedimentation of the suspension surface becomes quite noticeable, figure 4(*e*), (*f*). The bright patches now extend a considerable distance below the suspension surface ($\sim$1 cm) and form what we term 'streamers'. These streamers sink rapidly into the suspension, figures 4(*h*), (*i*), triggering the rapid settling of the gel. Upon reaching the bottom, the streamers destroy the layer of bright material by mixing, figure 4(*o*). Streamers have a tendency to travel down the paths formed by earlier channels, figures 4(*f*)–(*h*). However, this is not always true as can be seen in figure 4(*n*) where a wide channel has broken through the suspension surface near its middle while the streamers still propagate from the upper corners of the sample. Small volcano-like features are observed on

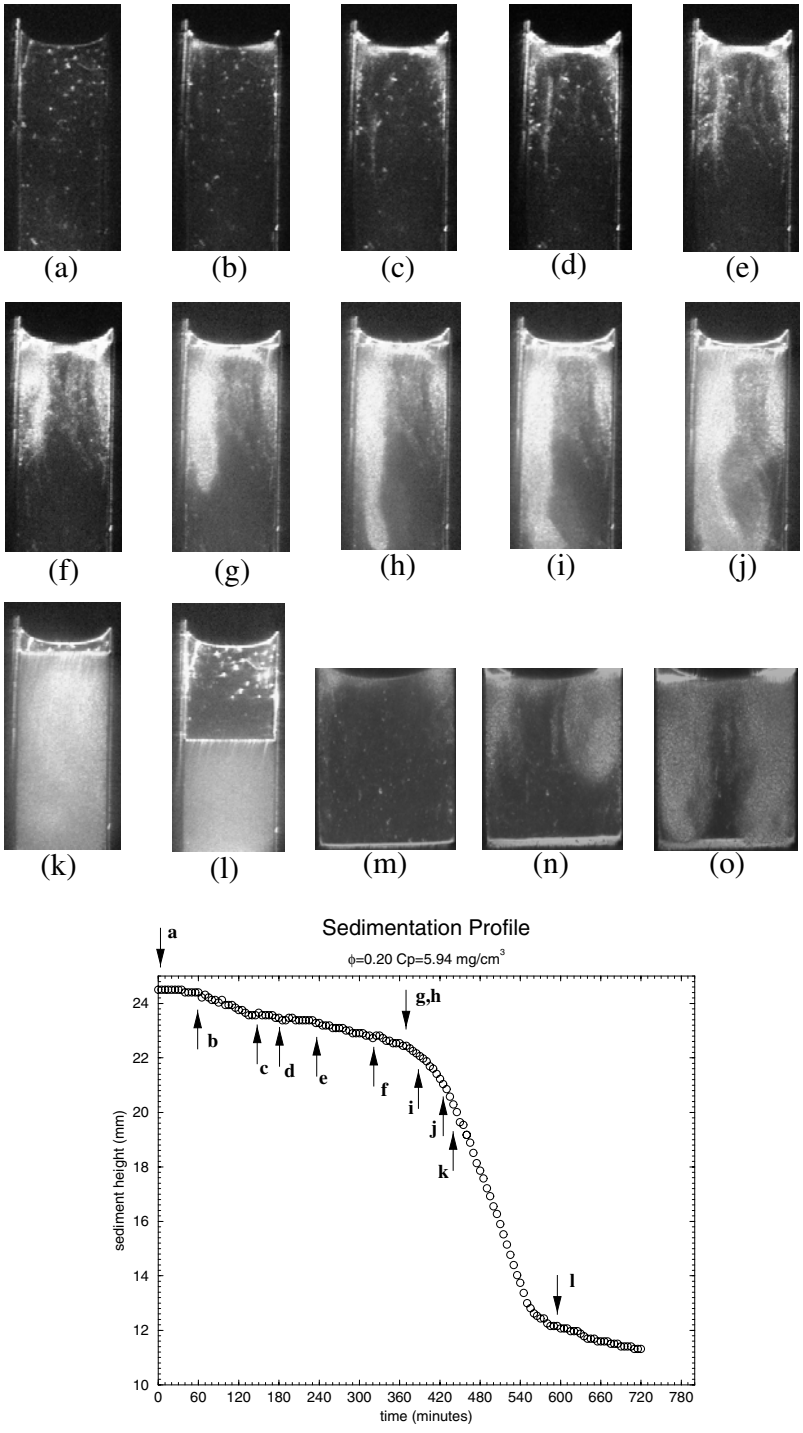

Figure 4. Dark-field images of a gel undergoing delayed sedimentation with a latency time of 420 min. For images (*a*)–(*l*) the time at which each image was captured is shown in the $h(t)$ plot for this sample. Images (*m*)–(*o*) show what happens at the bottom of a sample during delayed sedimentation. Here the latency time was 200 min and the images were captured at 60, 150 and 180 min respectively. An animated GIF of this figure is available (2.5 MB).

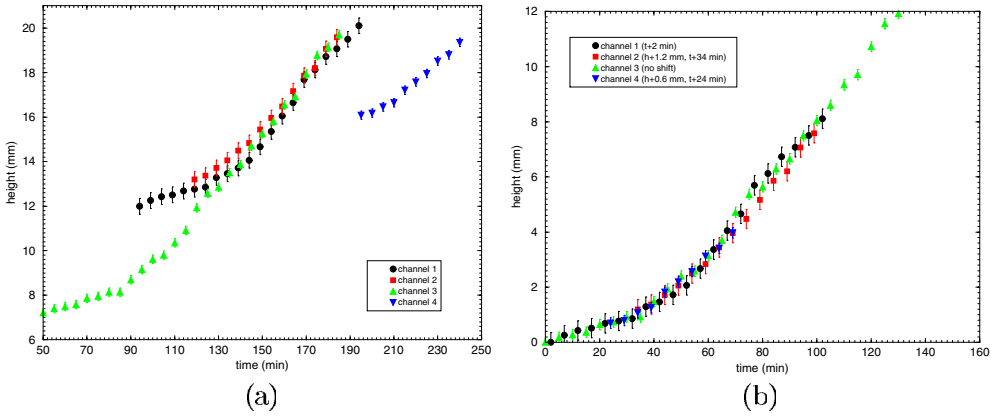

Figure 5. (*a*) Graph of channel height against time for a gel showing delayed sedimentation with delay time $\tau \approx 460$ min ($\phi = 0.20$, $C_p = 5.94$ mg cm^{-3}). (*b*) Graph of shifted channel height against time for the same data set as in (*a*).

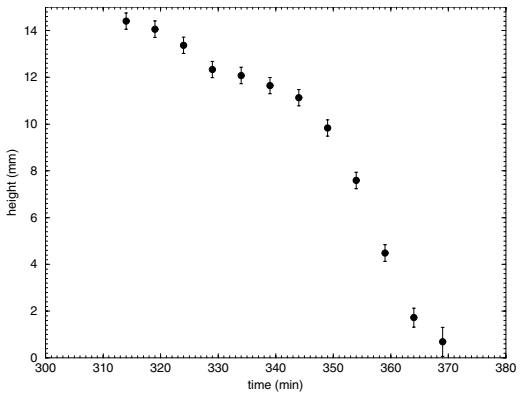

Figure 6. Graph of streamer height against time for a gel showing delayed sedimentation with delay time $\tau \approx 460$ min ($\phi = 0.20$, $C_p = 5.94$ mg cm^{-3}).

the suspension surface above the streamers. These form due to the expulsion of solvent from the suspension which is causing some of the material on the surface to be forced upwards into the supernatant. The size and frequency of these volcano-like features rises dramatically moments before the streamer velocity suddenly increases indicating an increase in solvent expulsion from the suspension.

Figure 6 shows how the height of a streamer front varies with time in a sample with $\phi = 0.2$, $C_p = 5.94$ mg cm^{-3}, $\tau \approx 460$ min. The rate at which the streamers move through the sample increases rapidly as the end of the latency time approaches. Streamers initially move relatively slowly through the sample; however, at around $t = 348$ min the rate at which the streamer propagates suddenly increases signalling the onset of rapid collapse. The slow propagation velocity as determined from figure 6 ($v_s^{st} = 1.7$ μm s^{-1}) is of the same order of magnitude as the fast sedimentation rate v_f. The streamer's fast propagation velocity is ten times faster than v_f.

During the rapid sedimentation phase, figures 4(*k*), (*l*), circulation of material can be seen (not visible in still pictures). During this part of the settling process the fluctuation of speckles is

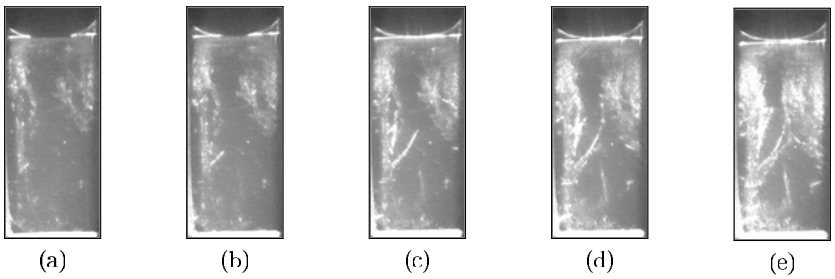

Figure 7. Dark-field images of a gel exhibiting delayed sedimentation with a delay time of 1000 min (10.5 h). Images (*a*) to (*e*) were captured at 360, 420, 480, 540 and 600 min respectively. The initial sample height is $h(0) = 20.8$ mm.

very rapid and slows down as the suspension settles. These speckles are caused by the partially coherent nature of the illumination source and are not a feature of the sediment. A region of slow speckle fluctuation is observed to grow upwards from the bottom of the cell during this time indicating the presence of dense sediment forming at the bottom as the suspension settles. A diffuse boundary between settling and compact suspension can be observed and measured. When the top sediment surface and the bottom compaction surface meet the rate of settling falls dramatically, figure 4(*l*).

Dark-field observations of delayed sedimentation in gels with long delay times show similar features to those of the shorter-lived gels. The formation of channels, bright bands and streamers are all observed. However, we also observe horizontal cracking of the suspension during the delay time. This can occur in the bulk region of the sample but frequently starts from the cell walls and propagates inwards and upwards into the sample. Cracks are different in appearance from channels. They are narrower and do not propagate directly upwards as the channels do. We also do not observe material being transported along cracks. The main features of long-delay-time gels are shown in figure 7 which shows a sequence of dark-field images captured during the delay stage from a gel with a delay time of 1000 min (10.5 h).

Figure 7(*a*) shows a crack that has just formed on the left-hand side of the sample at approximately one-third of the total sample height. This crack propagates into the sample as shown in figures 7(*b*)–(*d*). The very bright areas near the top of the sample indicate regions where many small cracks have formed. This region was so bright that it was difficult to see the formation of streamers although they were observed. Figures 7(*c*)–(*e*) show a channel moving upwards in the sample from an origin near the base. We also observe a bright band growing in thickness near the bottom. In this case the band reached a larger maximum thickness than was observed for shorter-lived gels and persisted after the onset of rapid collapse. We also observe a slower streamer propagation rate in comparison with the short-delay-time gels. During the rapid-collapse stage the circulation of material also appears slower than in the shorter-lived gels.

At the highest polymer concentrations a different settling behaviour is observed. The suspension continuously settles at a rate comparable to the initial slow setting rate of gels exhibiting delayed sedimentation and does not undergo a transition to a rapidly sedimenting stage. We have termed this kind of settling behaviour ‘creeping sedimentation’. The height against time plot for such a suspension as shown in figure 8 does not have the characteristic shape of delayed sedimentation.

Figure 8 shows a time-lapsed sequence of dark-field images for a sample which exhibits creeping sedimentation behaviour ($\phi = 0.20$, $C_p = 6.98\,\mathrm{mg\,cm^{-3}}$). Initially the sample

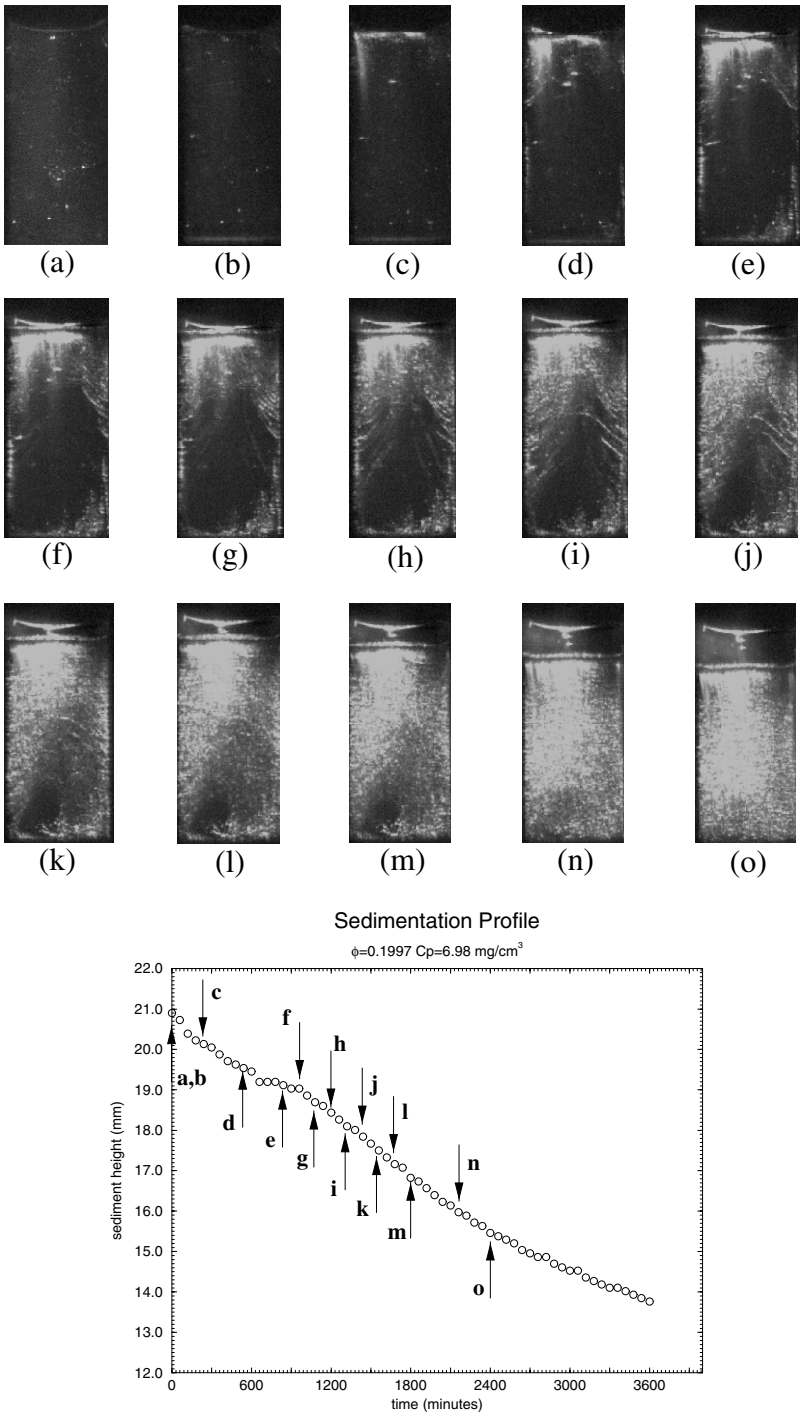

Figure 8. Dark-field images of a gel exhibiting creeping sedimentation behaviour. The time at which each image was captured is shown on the $h(t)$ plot. An animated GIF of this figure is available (3.5 MB).

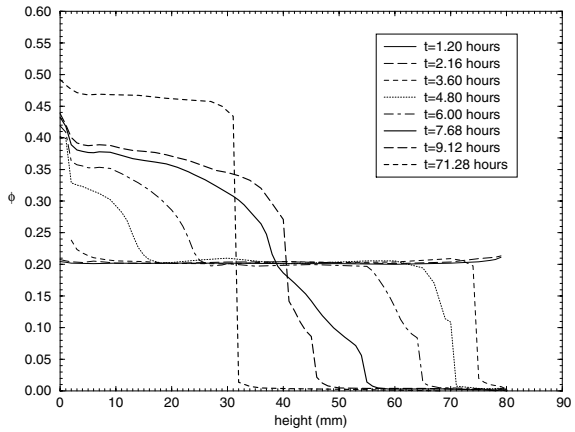

Figure 9. Concentration profile of a gel with a delay time of $\tau \approx 3$ h ($\phi = 0.19$, $C_p = 7.39$ mg cm^{-3}, $h(0) = 79$ mm).

appears dark except for small bright spots caused by dust on the cell walls. The suspension begins to slowly sediment almost immediately after the beginning of the experiment. A coarse, bright texture forms at the top of the sample at early times, figure 8(*b*), and moves downwards with time. Further down in the suspension, crack-like features grow inwards and upwards into the sample from the cell walls. These features move very slowly into the sample and are similar in appearance to those observed in long-delay-time gels, see figure 7. The cracks first appear near the top of the sample, figures 8(*d*)–(*e*), but as the suspension settles, they begin to form lower down, figures 8(*f*)–(*i*). Smaller cracks are also observed propagating horizontally far from the cell walls, for example figures 8(*d*)–(*f*). The cracks are finally broken up by the downward propagating bright texture, figures 8(*j*)–(*m*), which eventually fills the entire sample cell. These samples have been observed over a period of weeks and have shown no sign of rapid collapse. Samples with higher polymer concentrations show creeping behaviour with slower settling rates. Visual inspection of the bright region shows a granular texture as if it were composed of large aggregates. Large cracks open up in the sediment producing voids which are then filled by surrounding material. In the regions where no cracking is observed the sample appears smooth and undisturbed.

3.2. Concentration profiles

Direct observation of gels has given us some insight into the physical processes involved in the collapse process. In the images presented in the previous section we interpreted regions of brightness as indicating broken gel structure. This interpretation implies that these regions have more density inhomogeneities than the surrounding gel and can cause instability to propagate throughout the whole sample, for example streamer formation leading to global mixing of the gel in figure 4. Using the non-intrusive ultrasonic technique as described in section 2, we have measured the concentration of colloid–polymer gels during the collapse process. We now present the results of this study.

Figure 9 shows a plot of colloid volume fraction against height in the suspension for a gel with a delay time of 3 h ($\phi = 0.19$, $C_p = 7.39$ mg cm^{-3}, $h(0) = 79$ mm). The curves on this plot represent the concentration of the gel as a function of height at successive times. Initially the sample has a homogeneous concentration of $\phi \approx 0.20$. The concentration profile remains

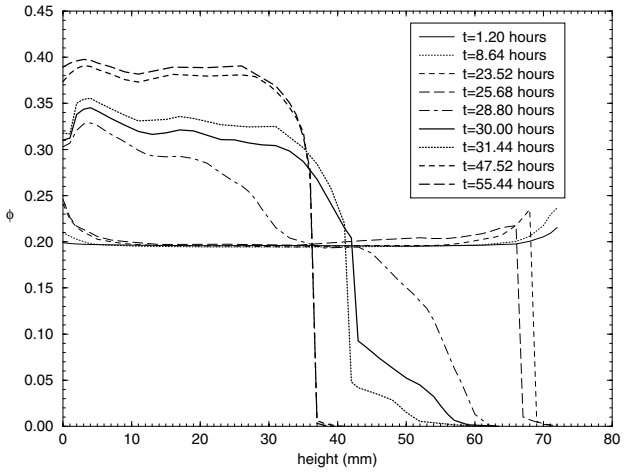

Figure 10. Concentration profiles of a long-delay-time gel, $\tau \approx 25$ h ($\phi = 0.19$, $C_p = 10.66$ mg cm^{-3}, $h(0) = 55$ mm).

unchanged throughout the delay time although small rises in concentration are observed at the very top and bottom of the suspension. These features are difficult to see in short-lived gels as they are small ($\Delta\phi \sim 0.01$) but are larger in gels with longer lifetimes ($\Delta\phi \sim 0.05$).

By $t = 3.6$ h the gel has entered the rapid-collapse stage. This is marked by the appearance of a sharp interface at the top ($h = 74$ mm) between the colloid-rich suspension and the colloid-poor supernatant. The concentration above this sharp interface falls to zero indicating that no colloidal material is left behind as the gel collapses. The concentration gradually increases towards the bottom of the sample over the space of 1 cm while the bulk of the suspension remains homogeneous in concentration at the original volume fraction.

As time progresses the top boundary continues to fall, $t = 4.80$–6.00 h. Although this boundary remains sharp, we observe a gradient in concentration forming and growing in thickness underneath it. Immediately below this first region of concentration gradient there is a thick layer of material which maintains the original concentration. Below this, a thick layer of dense sediment builds up from the bottom. The sediment concentration decreases over a height of 1 cm at its top. After 8 h the sample has developed a concentration gradient throughout its entire height. The interface between the dense sediment and the suspension above it is very diffuse at first. However, as settling proceeds this interface sharpens and moves upwards in the sample. Eventually, after 72 h, we observe a very sharp interface between colloidal sediment and supernatant. The dense sediment continues to slowly compact under its own weight becoming more uniform in concentration.

The concentration profiles of long-delay-time gels show many features similar to those observed for much shorter-lived gels. Figure 10 shows the concentration profiles for a gel with a delay time of 25 h ($\phi = 0.19$, $C_p = 10.66$ mg cm^{-3}, $h(0) = 71$ mm). The suspension is initially homogeneous at a volume fraction of around 0.2 and remains so throughout the delay time. We observe clear rises of up to 0.04 in the top and bottom few millimetres during the delay time while the bulk of the suspension remains unchanged. We also observe the formation of a sharp interface between colloid and supernatant at the top before the onset of rapid collapse signalling that this sample has settled below the base of the meniscus before the onset of rapid collapse.

Near the end of the rapid-collapse stage the concentration profile has a shape similar to that of the shorter-lived gels at a similar point in their collapse, for example $t = 6$ h in the 3 h

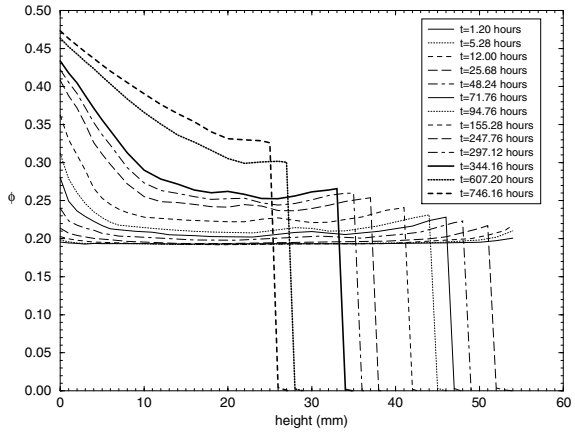

Figure 11. Concentration profiles of a gel exhibiting creeping sedimentation ($\phi = 0.19$, $C_p = 10.66$ mg cm^{-3}, $h(0) = 71$ mm).

gel. Large oscillatory fluctuations are observed throughout the dense sediment. The largest of these occurs at the very bottom where the concentration appears 2–3% lower than it is 5 mm higher up in the sample. These features become less pronounced as the sediment compacts. The origin of these features is unknown.

The concentration profile of a gel exhibiting creeping sedimentation shows features very different to those of delayed sedimentation as shown in figure 11. In order to obtain creeping behaviour we have studied the previous sample ($\tau = 25$ h) but have only filled the sample cell to a height of 55 mm. The effect of sample height on the collapse of transient gels will be discussed in more detail later and is treated theoretically in the following companion article [19].

Initially the suspension has constant, homogeneous concentration ($\phi \approx 0.2$). During the first 12 hours only the top and bottom few millimetres increase in concentration slightly while the bulk of the suspension maintains the original concentration. After one day, a sharp interface is clearly observed at the top of the settling suspension separating it from the clear supernatant left on top. Over the next 30 days the suspension continues to sediment slowly. A gradient in concentration begins to form at the bottom of the suspension. This denser sediment merges into a region of constant concentration above it in a smooth manner. As the boundary settles the whole suspension becomes gradually more concentrated while maintaining the shape of the profile. The layer of concentration gradient grows in thickness until it almost fills the whole of the sample after 31 days.

Some small oscillatory fluctuations begin to form in the middle of the sediment after 2 days. These grow a little in amplitude and move downwards in the suspension over the next 12 days but have disappeared after 25 days of settling. Even after 1 month we note that this sample has not yet finished settling nor has it shown any evidence that it may undergo a rapid collapse.

3.3. Sedimentation profiles: height and width dependence

We now present the results of a study of height- and width-dependent delay times. It has been found that the delay time of a transient gel can depend upon the initial height and width of the sample [18, 19]. Previously it was thought that only gels with strong depletion interactions

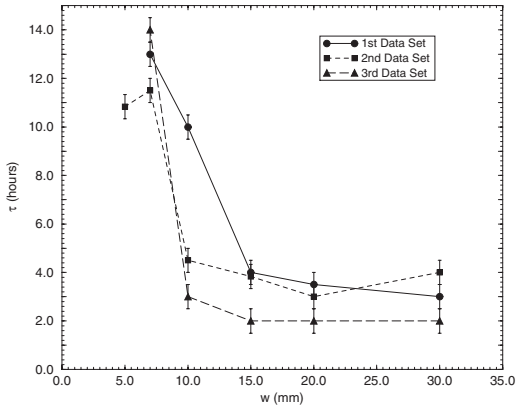

Figure 12. Plot of delay time τ against sample width for a gelled sample of initial height $h(0) = 20$ mm ($\phi = 0.20$, $C_p = 7.14$ mg cm^{-3}) .

showed size-dependent delay times while the weaker gels showed no such effect [18]. However, theoretical work [19] predicts the existence of a characteristic stress transmission lengthscale above which the gel should have size-independent properties (including delay time) and below which size-dependent properties may be observed.

In order to test the predictions of this theory, we measured the sedimentation profile of a colloid–polymer gel of composition $\phi = 0.20$, $C_p = 7.14$ mg cm^{-3} in a wide range of sample heights and widths. From our data we have found regimes of sample height and width where the delay time is independent of size, and other regimes where the size of the gel affects the delay time. We found a width-independent delay time above an initial sample width of 10 mm when the sample height was held fixed at 20 mm, see figure 12. For wide samples, the average delay time of the gel asymptotes to about 180 min, but sharply increases for widths less than about 10 mm. These observations suggest that, for a sufficiently tall sample, there exists a characteristic width $w_c \approx 10$ mm below which the delay time is dependent on the width of the sample.

When the suspension width was fixed at a value far larger than 10 mm, we found that the delay time was height-independent for samples taller that 5 mm ($\tau \approx 180$ min). The delay time sharply increased when the initial sample height was equal to 5 mm, see figure 13. It was not possible to study heights lower than this due to large meniscus effects. Our observations suggest that, for sufficiently wide samples, there exists a characteristic height h_c below which the delay time becomes dependent upon sample height. For this sample $h_c \approx 5$ mm.

It is noticeable that the delay time of the gel saturated at a value of around 180 min when it had dimensions much greater than its characteristic height or width. Another noticeable feature was the variation in relative uncertainty on the delay time as the size of the sample changed. Previously [15, 18] it was observed that the delay time of a particular gel was subject to a 20% scatter due to random processes, the origins of which are unknown but are intrinsic to the gel network. However, in the present study we have found that the variation in measured delay time depends upon how close in height and width the sample is to its characteristic size. In particular we have found that the delay time of a gel close to 1 cm in height and width is highly irreproducible carrying an uncertainty of up to 85%, for example $\tau(h = 20$ mm, $w = 10$ mm$) = 335 \pm 250$ min and $\tau(h = 10$ mm, $w = 10$ mm$) = 400 \pm 340$ min.

We have also found that the initial sedimentation rate of a gel in the height- and width-independent regime is zero as indicated by a flat region in the sedimentation profile, see

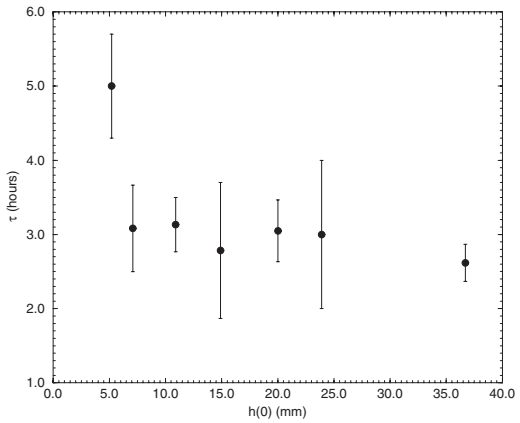

Figure 13. Plot of average delay time $\bar{\tau}$ against initial sample height $h(0)$ for a gelled sample of width 30 mm ($\phi = 0.20$, $C_p = 7.14$ mg cm^{-3}).

figure 14(*a*). This is contrary to what has been found previously [15, 18, 27] (also see the sedimentation profile in figure 4). A non-zero value for the initial sedimentation rate, v_s, was only found once the height or the width became comparable to the characteristic width, i.e. 1 cm. This may be explained by considering the shape of the sample meniscus. All the samples that we have studied have had a solvent–air interface at the top and thus a meniscus. When the width of the sample exceeds about 1 cm, the meniscus is almost flat. When the meniscus is flat the gel adheres to it via the depletion force. This stretches the gel structure near the top but does not easily tear it from the meniscus. In this way, the sedimentation of the gel is prevented until the onset of rapid collapse. These wide samples are the ones which exhibited zero initial settling rate. Conversely, when the sample cell is narrower, as it is in most cases, the meniscus is highly curved. A curved meniscus allows slippage of the gel from the top corners. This drainage helps the gel detach from the meniscus thus removing any support from above, and we observe draining of colloidal material from the edges of the meniscus, from the earliest times. Once the support from the top surface has been removed, the gel can begin to sediment. As a further justification for our proposal we note that zero initial sedimentation is observed when a sample cell is completely filled so as to remove the meniscus, effectively replacing a curved meniscus with a flat top surface [18]. Also transient gels formed from oil-in-water emulsions show no initial slow creaming before the onset of rapid creaming [28]. These emulsion gels have a completely flat bottom surface, equivalent to our top surface, as they cream from the bottom of the cell to the top.

When, for the same composition, the sample container was made very short and narrow ($h(0) = 10$ mm, $w = 7$ mm) we observed creeping sedimentation, figure 15. Thus creeping behaviour not only arises due to strong enough interparticle potentials but can also be due to placing a gel in a small enough container ($h(0) \ll h_c$, $w \ll w_c$). In this way creeping behaviour may be viewed as extreme size dependence [19].

4. Discussion

In the previous section we presented a series of observations of gel collapse in a model colloid–polymer system. In carrying out this study we have uncovered new information on the way in which transient gels collapse. However, we are no nearer to formulating a quantitative

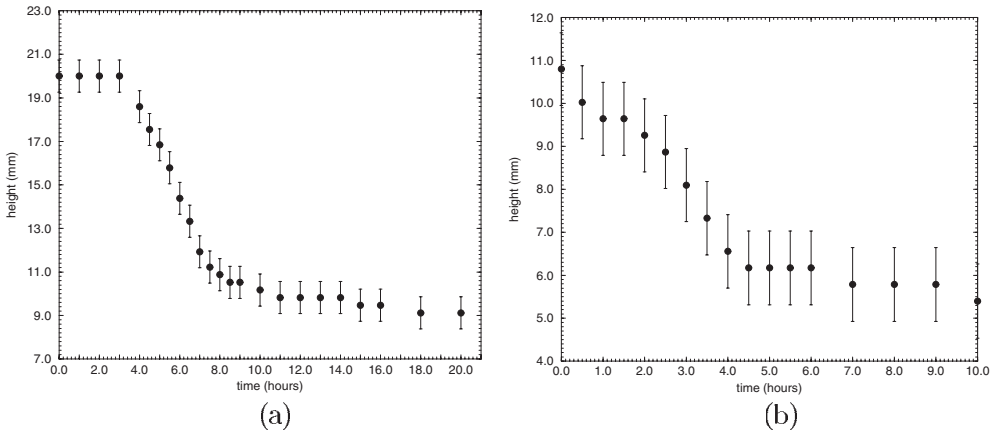

Figure 14. (*a*) A sedimentation profile for a gel whose dimensions are larger than the characteristic length scale ($h(0) = 20$ mm, $w = 30$ mm). The initial slope of the profile is flat. (*b*) The same gel in a cell of dimensions $h(0) = 10$ mm and $w = 7$ mm. In this case the gel does show some initial slow settling.

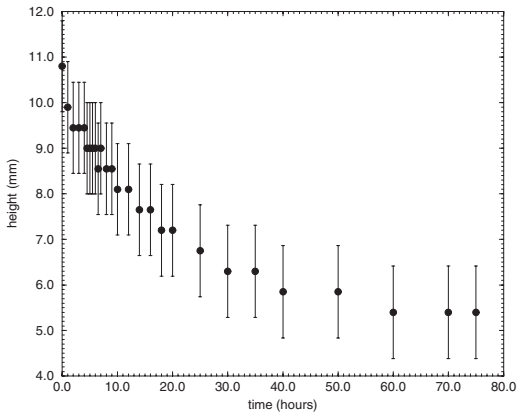

Figure 15. Sedimentation profile showing creeping sedimentation in a 7 mm wide sample ($\phi = 0.20$, $C_p = 7.14$ mg cm^{-1}).

model to describe the fundamental processes involved. We have found two different types of settling behaviour. At low and intermediate polymer concentration above the gel boundary we found gels which undergo delayed sedimentation. At high enough polymer concentration the settling behaviour changes and rapid collapse was no longer observed. This behaviour was termed creeping sedimentation and was also found to be an effect of making the sample dimensions much smaller than some characteristic size intrinsic to the gel. During the delay time the concentration remained constant and homogeneous throughout almost the whole height of the sample. This suggests that whatever physical processes may be responsible for the weakening and collapse of the gel must occur homogeneously throughout the particle network. Interestingly, we observed a variety of new macroscopic features in the gel during the delay time, a period in which the gel was previously believed to be dormant on the macroscopic level. These features, such as channelling and streamer formation, cause local breaking of the gel but do not trigger immediate large-scale collapse suggesting that the gel can initially support

such local macroscopic restructuring. We now focus on each of these new features and discuss the implications for further theoretical work suggested by our study.

Channels are direct routes for solvent to reach the surface of the slowly settling gel. They appear as bright objects in dark field due to the breaking of the surrounding particle network caused as the solvent pushes upwards. We have also observed colloidal material moving upwards in these channels which presumably has been torn from the gel structure by the flowing solvent. Channel-like features have been reported in other systems which display delayed sedimentation [1, 17]. Glasrud *et al* [17] attribute the formation of channels in sedimenting suspensions of iron oxide to small air bubbles entrained in the suspension by mixing. These channels then filled with the suspending oil. In the case of aqueous suspensions of calcium carbonate [1], the onset of rapid collapse has been attributed to the formation of a fracture in the suspension which provides the water with a route to the surface [29]. Neither of these channel formation mechanisms appears appropriate to our system.

Channel formation in our system may be a result of flow-induced rearrangement of the particle network. The interconnected porous structure of a gel forms a network of microscopic channels as may be demonstrated by two-dimensional reversible DLCA simulation [7]. Solvent may flow through these micro-channels choosing the path of least resistance to reach the suspension surface. This flow of solvent may erode non-percolating material from the surface of the particle network thus widening the micro-channels. The increasingly rapid flow of solvent may break off material from the channel walls, increasing the channel width further. In fact, it is the breaking of the gel at the channel edges that renders them visible in dark field. We have also observed that the macroscopic channels carry fragments of broken gel to the surface of the gel. The plot of channel height with time displays a shape that is consistent with the presence of a positive feedback loop of ever increasing solvent flow and channel widening. Initially channels propagate at a rate of around 0.5 μm s^{-1}. This sharply increases to around 2 μm s^{-1} about 50 min after the first sighting of the channel, see figure 5(*b*). It is interesting to note that the shape of the channel height against time curve does not depend on where or when the channel forms suggesting that, at least macroscopically, the material properties of the gel do not significantly change through the delay time. It would be a theoretical challenge to predict the shape of the master curve shown in figure 5(*b*).

Interestingly, we have found that transient gels always destabilize from the top forming streamer-like features which trigger large-scale flow and mixing of the sample. Our dark-field observations imply that regions of non-uniform concentration form at the top of the gel. This was confirmed by the concentration measurements which showed a small rise in average concentration in the region where the streamers first formed. Why the gel structure should begin to break from the top is unclear although one possible explanation may be that macroscopic channels deposit broken gel fragments on the top of the suspension once they have broken through the surface. This more compact, and therefore more concentrated, material may then sink into the surrounding gel causing local breaking and flow of the particle network. It is clear from our observations that the streamer features are the triggering mechanism for large-scale collapse of the gel. It is the rapid propagation of the streamers into the bulk of the sample that causes the observed large-scale circulation which culminates in the collapse of the gel. However, we can still only speculate on the physical processes behind their formation and propagation. What is clear is that the gel network is able to tolerate such macroscopic disturbances in its structure for only a finite period of time.

At high enough polymer concentration we have observed cracking of samples which undergo delayed sedimentation. These cracks predominantly formed at the cell wall and propagated into the bulk, see figure 7, suggesting that significant stresses are imposed on the gel by the wall. These stresses can play an important role in supporting the gel structure and

form the basis of a theoretical model that predicts the appearance of size-dependent properties below a certain lengthscale characteristic of the transient gel network [19].

By studying the effect of varying the height and width of a gel on its delay time, we found evidence for the existence of a characteristic lengthscale as predicted [19]. We found that a transient gel may show size-dependent or size-independent delay times according to its initial height and width. There exists a lengthscale characteristic of the gel above which its properties, including the delay time, do not depend upon the initial height and width of the sample. Conversely, gels that are smaller than this lengthscale show delay times which are sensitive to size. We also found that the characteristic height of a gel was about half of the characteristic width, $2h_c \simeq w_c$. The origin of this lengthscale is explained by the model described in the following article [19]. This model predicts the existence of a lengthscale beyond which stresses may not be transmitted in a gelled network. In the absence of stresses being transferred from the cell walls and base, the gel settles at a terminal velocity. However, if stresses are transmitted to the bulk then the gel may be supported by the walls and base leading to size-dependent properties. The theoretical prediction of the characteristic lengthscale for a gel with $\phi = 0.20$, $C_p = 7.14$ mg cm^{-3} is consistent with our findings of a crossover width of 10 mm and height of 5 mm [19].

One final point to consider is the existence of a different type of settling behaviour found at the highest polymer concentrations. It is clear from both dark-field observation and concentration measurements that creeping sedimentation shows none of the features observed in delayed sedimentation. In particular, samples undergoing creeping sedimentation do not lose their structural integrity in such a dramatic way as those which show delayed sedimentation. Our concentration profiles suggest that these samples compress more or less uniformly under their own weight. We also do not observe any of the local disruptions to the structure such as channels and streamers in samples that creep. By studying the effect of sample height and width on the delay time we have shown that creeping sedimentation may be an effect of extreme size dependence [19].

5. Conclusion

In this paper we have presented the findings of a study into the collapse of transient gels. Our motivation was the need for more information on the collapse process and we have found many, previously unreported features of this phenomenon. However, the aim of formulating a theory of gel collapse is still a distant goal and presents a challenging problem. The formation of transient gels has been extensively studied in recent times [2,5,7–10] and remains a subject for debate. Only now has a theoretical model been developed that describes the very early stages of gel collapse [19]. From this model, it is apparent that the properties of a transient gel are fixed from the earliest times after formation. In particular, the presence of a characteristic stress transmission lengthscale, set by the bulk properties of the gel, may account for the appearance of height- and width-dependent delay times that have been observed in this study. Although theoretical progress has been made, there remain many challenges to the formation of a comprehensive model of gel collapse. Most obviously, we are still unable to predict the delay time of a transient gel; however, there are many other features of the late stages of gel collapse that we may wish to predict. The formation and growth of the channel- and streamer-like features as observed in dark field remain unexplained as do some features of the concentration profiles of collapsing gels. It would be interesting to be able to predict the shape of the channel height against time curve, figure 5.

Acknowledgments

LS would like to thank the EPSRC and the Institute of Food Research for a CASE award. MR and DH acknowledge the BBSRC and the Institute of Food Research for financial support. We are grateful to R M L Evans and S Meeker for useful discussion and to Andrew Schofield for providing the colloidal material used in this study.

References

[1] Allain C, Cloitre M and Wafra M 1995 *Phys. Rev. Lett.* **74** 1478
[2] Poon W C K, Pirie A D and Pusey P N 1995 *Faraday Discuss.* **101** 65
[3] Parker A, Gunning P A, Kim Ng and Robins M M 1995 *Food Hydrocolloids* **9** 333
[4] Verhaegh N A M, Asnaghi D, Lekkerkerker H N W, Giglio M and Cipeletti L 1997 *Physica* A **242** 104
[5] Grant M C and Russel W B 1993 *Phys. Rev.* E **47** 2606
[6] Segré P N, Prasad V, Schofield A B and Weitz D A 2001 *Phys. Rev.* E **86** 6042
[7] Haw M D, Sievwright M, Poon W C K and Pusey P N 1995 *Adv. Colloid Interface Sci.* **62** 1
[8] Soga K G, Melrose J R and Ball R C 1998 *J. Chem. Phys.* **108** 6026
[9] Bergenholtz J and Fuchs M 1999 *Phys. Rev.* E **59** 5706
[10] Bergenholtz J, Fuchs M and Voigtmann Th 2000 *J. Phys.: Condens. Matter* **12** 6575
[11] Asakura S and Oosawa F 1958 *J. Polym. Sci.* **33** 183
[12] Lekkerkerker H N W, Poon W C K, Pusey P N, Stroobants and Warren P B 1992 *Europhys. Lett.* **20** 559
[13] Poon W C K, Selfe J S, Robertson M B, Illet S M, Pirie A D and Pusey P N 1993 *J. Physique* **3** 1075
[14] Vicsek T 1994 *Fractal Growth Phenomena* (Singapore: World Scientific)
[15] Poon W C K, Starrs L, Meeker S P, Moussaïd A, Evans R M L, Pusey P N and Robins M M 1999 *Faraday Discuss.* **112** 143
[16] Verhaegh N A M, Asnaghi D and Lekkerkerker H N W 1999 *Physica* A **264** 64
[17] Glasrud G G, Navarrete R C, Scriven L E and Macosko C W 1993 *AICE J.* **39** 560
[18] Meeker S P M 1997 *PhD Thesis* University of Edinburgh
[19] Evans R M L and Starrs L 2002 *J. Phys.: Condens. Matter* **14** 2507
[20] Berry G C 1966 *J. Chem. Phys.* **44** 4550
[21] Lipson S G, Lipson H and Tannhauser D S 1995 *Optical Physics* (Cambridge: Cambridge University Press)
[22] Pluta M 1988 *Advanced Light Microscopy* (Amsterdam: Elsevier)
[23] Howe A M and Robins M M 1990 *Colloids Surf.* **43** 83
[24] Hibberd D J 1997 *PhD Thesis* University of East Anglia
[25] Kaye G W C and Laby T H 1996 *Table of Physical and Chemical Constants* 14th edn (London: Longmans Green)
[26] Urick R J 1947 *J. Appl. Phys.* **18** 983
[27] Starrs L 1999 *PhD Thesis* University of Edinburgh
[28] Manoj P, Fillery-Travis A J, Watson A D, Hibberd D J and Robins M M 1998 *J. Colloid Interface Sci.* **207** 283
[29] Wafra M 1994 *PhD Thesis* Universitë Paris XIII